Published in final edited form as:
Cancer Res. 2010 April 15; 70(8): 3140–3149. doi:10.1158/0008-5472.CAN-09-4456.

Oncogenic Role of *miR-483-3p* at the *IGF2/483* Locus

Angelo Veronese[1,3], **Laura Lupini**[1], **Jessica Consiglio**[3], **Rosa Visone**[3], **Manuela Ferracin**[1], **Francesca Fornari**[2], **Nicola Zanesi**[3], **Hansjuerg Alder**[3], **Gemma D'Elia**[4], **Laura Gramantieri**[2], **Luigi Bolondi**[2], **Giovanni Lanza**[1], **Patrizia Querzoli**[1], **Adriano Angioni**[4], **Carlo M. Croce**[1,3], and **Massimo Negrini**[1]

[1]Dipartimento di Medicina Sperimentale e Diagnostica, Università di Ferrara, Ferrara, Italy

[2]Dipartimento di Medicina Interna e Gastroenterologia, Università di Bologna, Bologna, Italy

[3]Department of Molecular Virology, Immunology, and Medical Genetics, Ohio State University, Columbus, Ohio

[4]Ospedale Bambin Gesù, IRCCS, Struttura Semplice di Citogenetica e Genetica Molecolare, Rome, Italy

Abstract

hsa-mir-483 is located within intron 2 of the *IGF2* locus. We found that the mature microRNA (miRNA) *miR-483-3p* is overexpressed in 100% of Wilms' tumors. In addition, colon, breast, and liver cancers exhibit high or even extremely high levels of *miR-483-3p* in ~30% of the cases. A coregulation with *IGF2* mRNA was detected, although some tumors exhibited high expression of *miR-483-3p* without a concomitant increase of *IGF2*. These findings suggested that *miR-483-3p* could cooperate with *IGF2* or act as an autonomous oncogene. Indeed, here we prove that an anti-miRNA oligonucleotide against *miR-483-3p* could inhibit the miRNAs without affecting *IGF2* mRNA and it could suppress tumorigenicity of HepG2 cells, a cell line that overexpresses *miR-483-3p* and *IGF2*. Conversely, no antitumor effect was elicited by inhibition of *IGF2*. The oncogenic mechanism of *miR-483-3p* was at least partially clarified by the finding that it could modulate the proapoptotic protein *BBC3*/PUMA and *miR-483-3p* enforced expression could protect cells from apoptosis. Our results indicate that *miR-483-3p* could function as an antiapoptotic oncogene in various human cancers and reveal a new, potentially important target for anticancer therapy.

Introduction

Genetic and epigenetic abnormalities at chromosomal region 11p15.5 have been detected in various human neoplasms and in the cancer-predisposing Beckwith-Wiedemann syndrome. In particular, loss of alleles and gene duplication at 11p15 are typically detected in more

Corresponding Author: Massimo Negrini, Dipartimento di Medicina Sperimentale e Diagnostica, Università di Ferrara, via Fossato di Mortara, 70, presso "Il Cubo"-Piano 2, 44121 Ferrara, Italy. Phone: 39-0532-455399; Fax: 39-0532-455875; ngm@unife.it..

Disclosure of Potential Conflicts of Interest No potential conflicts of interest were disclosed.

Note: Supplementary data for this article are available at Cancer Research Online (http://cancerres.aacrjournals.org/).

than 80% of Wilms' tumors (1–5) and, albeit less frequently, in more common adult neoplasms (6–9).

Two close imprinted loci, which harbor at least eight monoallelically expressed genes, are present at chromosome region 11p15.5. The aberrant regulation of genomic imprinting at 11p15.5 was involved in human cancer (10–12). Aberrant methylation at the *H19* maternal locus leads to the reactivation of the silent *IGF2* allele (10, 13–16) and the loss of maternal allele methylation at the *KvDMR1* locus was linked to reduced expression of the cyclin-dependent kinase inhibitor *CDKN1C/*p57 gene and other imprinted genes (11, 12, 17–19). These studies point to the existence of oncogenic, *IGF2*, as well as tumor-suppressive, *CDKN1C/*p57, functions within the 11p15.5 chromosomal imprinted region.

IGF2 is a fetal growth factor, the abnormal expression of which has been involved in the Beckwith-Wiedemann syndrome, which predisposes to the development of nephroblastoma, hepatoblastoma, and rhabdomyosarcoma. Biallelic expression of *IGF2* gene, consequent to the loss-of-imprinting at the *IGF2* locus, occurs in 40% to 50% of Wilms' tumors (5, 20), and it is thought to be an early event in carcinogenesis. Therefore, it has been suggested that increased IGF2 could lead to an enhanced cellular proliferation, differentiation failure, and tumor development. However, a transgenic mouse model for *IGF2* overexpression exhibited many of the features associated with the Beckwith-Wiedemann syndrome, including prenatal overgrowth, polyhydramnios, fetal and neonatal lethality, disproportionate organ overgrowth including tongue enlargement, and skeletal abnormalities, but this mouse model did not develop tumors (21). These results suggest that additional cofactors should cooperate with IGF2 in promoting human cancer. Recently, the *IGF2* locus was shown to harbor a microRNA (miRNA), the *mir-483* locus, within its second intron (22).

In the last 7 years, the involvement of miRNAs in human cancer has been proved. Aberrant expression of miRNAs has been detected in any human neoplasm and miRNAs were found to play a central role in all molecular pathways affecting cancer traits (23–25). Recently, the role of the *miR-17-92* miRNA cluster in Wilms' tumors has been reported (26).

Here, we tested the potential oncogenic activity of *miR-483-3p*, one of the mature products at chromosome 11p15.5. Our results provide evidence for the role of this miRNA as an antiapoptotic oncogene involved in human tumorigenesis.

Materials and Methods

Primary tumors

Primary tumor RNAs were obtained from 19 Wilms' tumors, 3 adjacent patient normal tissues, 2 adult kidneys; 27 hepatocarcinomas, 7 cirrhotic, and 2 normal liver tissues; 23 colorectal cancers and 5 normal colon mucosa; 19 breast cancers and 4 normal breast tissues. All tissue samples were collected at surgery, immediately snap-frozen in liquid nitrogen, and stored at −80°C until RNA extraction. Total RNA was isolated using Trizol (Invitrogen) according to the instructions of the manufacturer.

Cell lines and transfection

HEK293, HepG2, and HCT116 cell lines (all from American Type Culture Collection) were cultured with Iscove's modified Dulbecco's medium with 10% fetal bovine serum. *hsa-miR-483-3p* precursor (Sanger accession no. MI0002467) and negative control 2 ribo-oligonucleotide were from Applied Biosystems/Ambion. Anti-miRNA oligonucleotides (AMO) against *miR-483-3p* and against the GFP gene (AMO Negative Control) were from Fidelity Systems. RNA interfering for *BBC3*/PUMA and scramble control were from Santa Cruz Biotechnology. Transfection of miRNAs, AMOs, and expression vectors was carried out with Lipofectamine 2000 (Invitrogen) in accordance with the procedures of the manufacturer.

Luciferase assays and vectors

The human 3′-untranslated region (UTR) of *BBC3*/PUMA was amplified by PCR using the primers indicated in Supplementary Table S1 and cloned downstream of the firefly luciferase gene in the pGL3-Control vector (Promega). Substitutions into the miR-483-3p binding sites of the *BBC3*/PUMA 3′UTR gene was introduced by using Quick-Change site-directed mutagenesis kit following the instructions of the manufacturer and using the primers indicated in Supplementary Table S1. As a reference, the pRLTK vector (Promega), which expresses the renilla luciferase, was used. Transfection was conducted in HEK293, HCT116, and HepG2 cells cultured in 24-well plates, each well was cotransfected with 400 ng of pGL3-control vectors together with 40 ng of pRLTK reference vector (Promega) and 30 pmol of *miR-483-3p* or negative control 2 or AMOs, or methylated control oligonucleotide. Twenty-four hours after transfection, *firefly* and *renilla* luciferase activities were measured using the Dual-Luciferase Report Assay (Promega).

Western blot analyses

HEK293 and HepG2 cell lines were transfected with 30 pmol of *miR-483-3p*, AMOs, and control sequences in 24-well plates. After 48 h, cells were collected, lysed in Laemmli 2× buffer, and analyzed by Western blot to assess the expression of PUMA using monoclonal antibodies (anti-PUMA antibody no. 4976; Cell Signaling). Primary antibody was incubated for 2 h at room temperature and then peroxidase-conjugated anti-mouse or anti-rabbit antibodies were incubated for 30 min at room temperature. Detection was conducted by chemiluminescent enhanced assay (WesternBreeze Chemiluminescent Kit; Invitrogen). β-Actin antibody (β-actin antibody no. 4976; Cell Signaling) or Ponceau staining were used to normalize protein loading. To quantify Western blot signals, digital images of autoradiographies were acquired with Fluor-S MultiImager, and band signals were quantified in the linear range of the scanner using specific densitometric software (Quantity One).

Quantitative real-time reverse transcription PCR

Mature miRNA expression was assayed by TaqMan MicroRNA assay (Applied Biosystems) specific for *miR-483-3p* (P/N: 4378094) and normalized on *RNU6B* (P/N: 4373381). Five nanograms of total RNA was reverse-transcribed using the specific looped primer and quantitative real-time reverse transcription PCR (qRT-PCR) was conducted using the

standard TaqMan MicroRNA assay protocol on a Bio-Rad-Chromo4 thermal cycler. The 20 μL PCR included 1.33 μL of reverse transcription product, 1× TaqMan Universal PCR Master Mix, No AmpErase UNG [P/N 4324018 (Applied Biosystems), 0.2 μmol/L TaqMan probe, 1.5 μmol/L forward primer, and 0.7 μmol/L reverse primer]. The reaction was carried out in a 96-well PCR plate at 95°C for 10 min followed by 40 cycles of 95°C for 15 s and 60°C for 1 min. Each sample was analyzed in triplicate. qRT-PCR for mRNA was performed using 500 ng of total RNA for each sample according to the instructions of the manufacturer (High-capacity cDNA Reverse Transcription Kit; Applied Biosystems) and the real-time reaction using SYBR green technologies (Power SYBR green PCR Master Mix; Applied Biosystems) on the Bio-Rad-Chromo4 instrument. The 20 μL PCR included 1 μL of reverse transcription product, 1× Power SYBR green PCR Master Mix (P/N 4368577; Applied Biosystems), 0.4 μmol/L forward primer, and 0.4 μmol/L reverse primer. The reactions were incubated in a 96-well PCR plate at 95°C for 10 min followed by 40 cycles of 95°C for 15 s and 60°C for 1 min. Each sample was analyzed in triplicate. TaqMan gene expression assays were performed for *IGF2*, *BBC3*/PUMA, and *CDKN1A*/p21 genes using primers and probes (Hs01005963_m1, Hs00248075_m1, and Hs99999142_m1) obtained from Applied Biosystems (Applied Biosystems). The expression of *18S* RNA was used as an endogenous reference control. The levels of miRNA and mRNA were measured using Ct (threshold cycle). The amount of target, normalized to an endogenous reference and relative to a calibrator, is given by $2^{-\Delta\Delta Ct}$ (comparative Ct method; Applied Biosystems User Bulletin no. 2).

Northern blot analysis

RNA samples (10 μg each) were electrophoresed on 15% acrylamide and 7 mol/L of urea Criterion precast gels (Bio-Rad) and transferred onto Hybond N+ membrane (Amersham Biosciences). Membranes were hybridized as previously described (27) with oligonucleotide probes corresponding to the complementary sequences of the mature miRNAs: *miR-483-3p* 5′-UCACUCCUCUCCUCCCGUCUU-3′ and the reference U6 RNA 5′-GCAGGGGCCATGCTAATCTTCTCTGTATCG-3′.

Cell death and cell viability assays

MTT assays were carried out on the HEK293 cell line. HEK293 was cultured in 24-well plates the day before *miR-483-3p* or AMOs transfection. After 24 h from transfection, cells were treated with doxorubicin (0.4 μg/mL) for an additional 24 h. The assay was performed in accordance with the protocols of the manufacturer (TOX-1; Sigma). Each experiment was performed in triplicate. Nuclear fluorescein staining based on labeling of DNA strand breaks by terminal deoxynucleotidyl transferase–mediated dUTP nick-end labeling reaction was performed on the HepG2 cell line according to the instructions of the manufacturer (*In situ* Cell Death Detection Kit; Roche). The experiment was performed in triplicate and analyzed on a Zeiss Axiovert 200 microscope at 100× magnification, images were acquired with the CCD Cascade Photometrics 512b. Quantification of positive nuclei was calculated by counting fluorescent spots in 10 images (10 × 10 magnifications) for each experiment. Caspase 3/7 activity assay was performed on HCT116 cell line. HCT116 was cultured in 96-well plates the day before *miR-483-3p*, AMO, and control transfection. After 24 h from transfection, cells were treated with Nutlin-3 (5 μmol/L) or 5-fluoruracil (from 0 to 50

μmol/L) for an additional 6 to 24 h, then the assay was performed in accordance with the protocols of the manufacturer (Caspase-Glo 3/7 assay, G8090; Promega).

Generation of stable cell lines overexpressing miR-483-3p and anti–miR-483-3p

HCT116 cells were infected with the PMIRH483 expression plasmid containing the full-length *miR-483-3p* and the GFP gene under the control of two different promoters (PMIRH483PA-1; System Biosciences). HCT116 and HepG2 cells were infected with the pSIH vector (System Biosciences) containing the antisense sequence for *miR-483-3p* (Supplementary Table S1) using the Lentivector-based anti-miRNA technology (miRZIP, System Biosciences). An empty vector was used as the control. Pre–*miR-483-3p*, anti–*miR-483-3p* expression, and control constructs were packaged with pPACKH1 Lentivector Packaging Plasmid mix (System Biosciences) in 293-TN packaging cell line. Viruses were concentrated using PEG-*it* Virus Precipitation Solution and titers analyzed using UltraRapid Lentiviral Titer Kit (System Biosciences). Infected cells were selected by fluorescence-activated cell sorting analysis (FACSCalibur, Becton Dickinson Immunocytometry Systems). An infection efficiency of >90% was verified by fluorescent microscopy.

In vivo *studies*

Animal studies were approved by institutional ethical committees. HepG2 cells were transfected *in vitro* with 2′-*O*-methyl RNA oligonucleotide complementary to *miR-483-3p* (anti-miR oligonucleotide: AMO-483-3p), AMO-Negative controls from Fidelity Systems, and small interfering RNA (siRNA) against the *IGF2* gene from Thermo-Scientific Dharmacon. At 24 h after the transfection, 10^7 viable cells per mouse were injected i.p. into 10 NOD-SCID mice (Charles River Breeding Laboratories). After 35 d, the mice were sacrificed, necropsies were performed, and all tumors per mouse were weighed. For athymic "nude" mice experiments, HepG2 cells (10×10^6 cells/200 μL) were injected s.c. into the flanks of nude mice 24 h after transfection with AMO-483-3p (four injections), AMO Negative Control (four injections), or siRNA IGF2 (six injections). Tumors were counted after 20 d.

Results

miR-483-3p is overexpressed in Wilms' tumor and common adult human cancers in concert with IGF2

Because of its location within the *IGF2* locus, we evaluated *miR-483-3p* expression in Wilms' tumor. Biopsies from 19 Wilms' tumors, 4 normal kidney tissues (three of which matched with Wilms' tumor samples), 1 fetal kidney, and 1 fetal liver as positive control were analyzed. Upregulation (from 4-fold to 40-fold) of miRNA expression was found in 73% of Wilms' tumors when compared with fetal kidney and in 100% of the cases when compared with non-tumoral kidney tissues (Fig. 1A and B). Northern blot analysis confirmed the qRT-PCR data (Fig. 1C).

Because *mir-483-3p* is located within the *IGF2* gene, we compared their levels of expression: a positive correlation between *IGF2* mRNA and *miR-483-3p* expression was found. By using two sets of primers spanning the junctions between exons 1 and 2 or exons

2 and 3 of the *IGF2* cDNA sequence, we found strong positive coefficients of correlation with *miR-483-3p* in both cases ($R = 0.94$, $P < 0.0001$ for product e, and $R = 0.60$, $P = 0.004$ for product f; Fig. 1D). These results indicate that the joint overexpression of at least two functional elements from the *IGF2* locus, the IGF2 protein and *miR-483-3p*, may act in Wilms' tumors to promote tumorigenesis.

We investigated the potential involvement of *miR-483-3p* in common human neoplasms. We analyzed the expression of *miR-483-3p* in breast, colon, and liver human cancers and we found that overexpression of *miR-483-3p* was indeed present, suggesting a wider involvement of this miRNA in human tumorigenesis. In primary colon, breast, and liver carcinomas (Fig. 2A–C), we compared the expression of *miR-483-3p* of tumors with the average expression of non-tumor histologic normal tissues. Considering the variability of *miR-483-3p* expression in non-tumor counterparts, only tumors exhibiting a fold-change of >10 in comparison with the average expression of non-tumor normal tissues were scored as overexpressed: 33% of hepatocarcinomas, 31% of breast, and 27% of colorectal cancers exhibited significant upregulation. Interestingly, cirrhotic liver tissues, a condition that predisposes to hepatocarcinoma, already exhibited an increased miR-483-3p expression (from 3-fold to 14-fold) when compared with normal liver tissues ($P < 0.05$; Fig. 2A).

We observed that, as in Wilms' tumors, the upregulation of *miR-483-3p* was linked with *IGF2* expression: a positive Spearman coefficient of correlation of 0.69 for hepatocarcinomas ($P < 0.0001$) and 0.86 for colorectal cancers ($P < 0.0001$; Fig. 2A and B). In spite of these significant positive correlations, some tumor samples (HCC_02, HCC_04, HCC_10, HCC_13, HCC_16, HCC_21, HCC_26, HCC_29, CRC_188, CRC_130, CRC_148) exhibited a divergent expression of *IGF2* and *miR-483-3p*, suggesting the existence of multiple mechanisms of *miR-483-3* upregulation.

miR-483-3p protects cells from apoptosis

To start unraveling the molecular basis of the potential oncogenic role of *miR-483-3p*, we focused on the apoptotic pathway because important proapoptotic human genes are predicted targets of miRanda and TargetScan algorithms (*BBC3*/PUMA, *AMID*, *BAX*, *BIK*, *SMAC*/DIABLO, *PDCD1*, and *PDCD7*). Thus, we evaluated apoptosis and cell viability in response to modulation of *miR-483-3p* in HEK293, HCT116, and HepG2 cells.

After treatment of HEK293 cells with doxorubicin to induce apoptotic cell death, transfection of *miR-483-3p* induced a low (10%) but significant increase in cell viability ($P = 0.05$), whereas transfection of anti–*miR-483-3p* AMOs induced a further 15% decrease in cell viability ($P = 0.02$; Fig. 3A). These results indicate that *miR-483-3p* could promote cell survival.

HepG2 cells express very high levels of *miR-483-3p*. Therefore, we evaluated only the effect of anti–*miR-483-3p* AMO in this cell line. Cell growth was inhibited 30% to 40% by transfection of anti–*miR-483-3p* AMO (Fig. 3B). Simultaneously, cells exhibited a 2.6-fold increase in the level of cell death compared with control cells transfected with a negative control AMO ($P = 0.016$; Fig. 3C), as detected by *in situ* cell death using fluorescent labeling of DNA strand breaks with terminal deoxynucleotidyl transferase.

To confirm that the mechanism was indeed apoptosis, caspase 3/7 activity was measured in HCT116 cells transfected with *miR-483-3p* or anti–*miR-483-3p* and treated with the apoptosis-inducing factor Nutlin-3A. Compared with the controls, caspase activity exhibited an 80% increase in anti-miR–treated cells and a 60% decrease in *miR-483-3p*–treated cells (Fig. 3D); moreover, we detected an inverse correlation between the amount of transfected *miR-483-3p* and caspase 3/7 activity, whereas a proportional increase was detected between AMO-483-3p and caspase 3/7 activity (Supplementary Fig. S2A).

PUMA is a target of miR-483-3p

In the list of potential proapoptotic target genes, the *BBC3*/PUMA (BCL2 binding component 3/p53 upregulated modulator of apoptosis) gene was chosen for further analysis because of its known pivotal role in induced cell death (28).

To test the direct interaction of *miR-483-3p* with 3′UTRs, the predicted wild-type and mutant *miR-483-3p* target sites of PUMA mRNA gene were cloned downstream of the luciferase reporter gene of pGL3-Control vector. The HEK293 cells were used as a biological system because they exhibited a low expression of *miR-483-3p*, HCT116 cells had medium expression, whereas the HepG2 cells exhibited a high expression of miR-*483-3p* (Supplementary Fig. S1A). Depending on the *miR-483-3p* expression, the *miR-483-3p* responsive vector was cotransfected with *miR-483-3p* into HEK293, either miR-*483-3p* or anti–*miR-483-3p* oligonucleotide (anti–483-3p AMO) into HCT116 cells and only anti–*miR-483-3p* into HepG2 cells (Fig. 4A). In comparison with control vectors, *miR-483-3p* induced a decrease in luciferase activity of ~38% (HEK293) and 45% (HCT116) of the pGL3 vector carrying the PUMA-3′UTR, whereas in the mutated 3′UTR clone, the luciferase activity was not significantly downregulated by *miR-483-3p*. Conversely, the use of anti–*miR-483-3p* AMOs induced an increase in luciferase activity of ~70% and 39% for HCT116 and HepG2 cells, respectively (Fig. 4B).

To further confirm PUMA as a target of *miR-483-3p*, its protein level was assessed by Western blot analysis on HEK293 and HepG2 cells transfected with *miR-483-3p* or anti–*miR-483-3p*, respectively. Protein expression was reduced (70%) in HEK293 and induced (40%) in HepG2 cells when compared with controls (Fig. 4C).

The analysis of two matched Wilms' tumors/normal kidney samples for the expression of PUMA protein revealed that, as predicted by the molecular function of *miR-483-3p*, the level of expression of these two proapoptotic proteins was significantly lower in tumors, in which *miR-483-3p* is expressed at higher levels (Fig. 4D).

To further support these data, we generated stable cell lines overexpressing the *miR-483-3p* or the anti–*miR-483-3p* to evaluate the expression of *BBC3*/PUMA after treatment with 5-fluorouracil (5FU) as an apoptosis-inducing factor that involves the p53 pathway. The HCT116 cells were infected with lentiviral vectors overexpressing *miR-483-3p* (LV-483) or anti–*miR-483-3p* (LV-AS483), whereas the HepG2 cell line was infected with LV-AS483. An empty vector was used as a control (LV-CTRL). The increased concentrations of 5FU matched with the increased PUMA protein levels only in the HCT116 and HepG2 cells overexpressing the anti–*miR-483-3p* (Fig. 5A), in spite of a homogeneous increment of

BBC3/PUMA mRNA levels (Supplementary Fig. S3A) in all stable cell lines. The induction of both *BBC3*/PUMA and *CDKN1A*/p21 mRNA levels by 5FU treatment suggests the activation of the p53 pathway (Supplementary Fig. S3A and S3B).

To assess the physiologic role of this finding, the caspase 3/7 activity of these stable cell lines was measured after 5FU treatment. Compared with controls, the HCT116-LV-483 cells showed a reduced caspase 3/7 activity (24–40%, $P < 0.0001$; Fig. 5B), whereas the HCT116-LV-AS483 cells exhibited an increased activity (4–28%, $P = 0.03$). As expected in HepG2-LV-AS483 cells, the caspase activity was also increased (21–70%, $P < 0.0001$; Fig. 5B). To further prove the connection between *miR-483-3p*, PUMA, and apoptosis, we proved that by knocking down PUMA using siRNA transfection, we could prevent the AS483-3p effect in HepG2-LV-AS483 cells (Fig. 5C). We used the HepG2 stable cell lines because the efficacy of anti–*miR-483-3p* was more evident than the HCT116 model (Fig. 5B).

AMO-miR-483-3p but not IGF2 siRNA can inhibit in vivo tumorigenicity

The potential oncogenic role of *miR-483-3p* was tested directly through tumorigenicity modulation of the human HepG2 cells, which overexpresses *miR-483-3p*. Twenty-four hours after the transfection of AMO-483-3p or siRNA anti-*IGF2* into HepG2 cells, qRT-PCR confirmed the specific reduction of *miR-483-3p* or *IGF2* mRNA, respectively (Fig. 6A). Then, 10×10^6 cells (cell viability greater than 97%) were i.p. injected into NOD-SCID mice. Mice were sacrificed on day 35 and all tumors for each mouse were weighed. The AMO-483-3p mouse group showed a significant reduction of number and weight of induced tumors compared with controls ($P < 0.05$). On the contrary, repression of the *IGF2* gene did not show any difference from controls ($P > 0.5$; Fig. 6B and C). The three groups of data (CTRL, AMO-483-3p, and siIGF2) were comparable because of the same nature of the molecules used to silence the *miR-483-3p* and *IGF2* gene (2′-O-methyl RNA oligonucleotide). Overlapping results were obtained by subcutaneous injections of HepG2 cells into athymic nude mice: AMO-483-3p induced a decrease in the number of growing tumors (one of four) in comparison with controls and *IGF2* siRNA (AMO-CTRL, four of four; siRNA anti-IGF2, four of six; Supplementary Fig. S4).

Discussion

We established a link between *miR-483-3p*, a miRNA located within the *IGF2* locus at chromosome 11p15.5, and human tumorigenesis. Various evidences support this conclusion. First, tumorigenicity of HepG2, a cell line that overexpresses *miR-483-3p*, is suppressed by AMO anti–miR-483-3p; second, miRNA is upregulated and overexpressed in Wilms' tumors as well as in common human neoplasms; third, *miR-483-3p* supports cell survival by protecting cells from apoptosis; fourth, an important regulator of apoptosis, Puma, is inhibited by the expression of *miR-483-3p*.

To show the oncogenic properties of *miR-483-3p*, we proved that silencing of *miR-483-3p* by AMO could reduce the tumorigenicity of HepG2 cells, a cell line that exhibits high expression of the *IGF2/miR-483* locus and functional activity of IGF2 ligand (29, 30). Importantly, the reduction in tumor formation by the specific silencing of *miR-483-3p* was

achieved without changing *IGF2* gene expression. Moreover, the silencing of the *IGF2* gene by siRNA technologies did not cause a significant change in tumor formation by HepG2 cells. These results clearly indicate that a crucial oncogenic function was associated with the *miR-483-3p* miRNA within the *IGF2* locus. This conclusion might explain why transgenic animal models for *Igf2* overexpression did not develop tumors (21). In fact, these animal models were developed by using an *Igf2* cDNA, which lacked the *mir-483* locus. It could be speculated that, by protecting cells from apoptosis, *miR-483-3p* provides the additional element required for supporting malignant transformation promoted by the growth factor IGF2. Indeed, in the Wilms' tumors, hepatocarcinomas, and colorectal cancers studied, the expression of the *IGF2/miR-483* locus is coregulated in almost all of the samples analyzed. Interestingly, some cases present divergent expressions of *miR-483-3p* and *IGF2*, suggesting a possible *IGF2*-independent mechanism of *miR-483-3p* regulation.

By proving that ectopic expression of *miR-483-3p* could protect cells from apoptosis, whereas inhibition of endogenous *miR-483-3p* increases basal or induced apoptosis, we show that the upregulation of *miR-483-3p* could protect cells from apoptosis. This is in line with the finding that *miR-483-3p* can target and repress the expression of the proapoptotic protein PUMA, a BH3-only protein, the induction of which is mediated by p53 (28, 31). Like other BH3-only proteins, it promotes apoptosis by interacting and inhibiting the antiapoptotic factors BCL2 and BCLXL (31–33). Hence, an overexpressed *miR-483-3p* might favor cell survival by reducing the level of Puma after p53 activation during apoptosis stimuli, and therefore acting as an antiapoptotic oncogene. Our results support this conclusion.

The involvement of *miR-483-3p* in cancer is supported by the observation that it is overexpressed in ~30% of common human cancers and in 100% of Wilms' tumors. In addition, Guled and colleagues reported the upregulation of *miR-483-3p* in malignant mesothelioma (34). In human cancers, the overexpression of *miR-483-3p* could be linked to its coregulation with *IGF2* expression. Interestingly, through this mechanism, both growth (IGF2) and survival stimuli (*miR-483-3p*) are simultaneously activated. However, some tumor samples displayed a divergent expression between *IGF2* and *miR-483-3p*, thus revealing the existence of mechanisms in which *IGF2* and *hsa-mir-483* are not coregulated. This is an area that needs further investigation.

The recent demonstration of the safe and effective use of anti-miRNAs in animal models, including African green monkeys, suggests the potential application of AMOs in anticancer therapy as well (35, 36). Our findings indicate *miR-483-3p* as a potential target for antineoplastic intervention in Wilms' tumors and possibly many other tumors. Thus, these results not only improve our understanding on the molecular mechanisms involved in tumor development, but they also provide an indication for a novel potential therapeutic target.

Supplementary Material

Refer to Web version on PubMed Central for supplementary material.

Acknowledgments

Grant Support Associazione Italiana per la Ricerca sul Cancro, Ministero dell'Università e della Ricerca, Ministero della Salute, and Fondazione Cariplo (Progetto NOBEL; M. Negrini).

References

1. Fearon ER, Vogelstein B, Feinberg AP. Somatic deletion and duplication of genes on chromosome 11 in Wilms' tumours. Nature. 1984; 309:176–8. [PubMed: 6325939]
2. Koufos A, Hansen MF, Lampkin BC, et al. Loss of alleles at loci on human chromosome 11 during genesis of Wilms' tumour. Nature. 1984; 309:170–2. [PubMed: 6325936]
3. Orkin SH, Goldman DS, Sallan SE. Development of homozygosity for chromosome 11p markers in Wilms' tumour. Nature. 1984; 309:172–4. [PubMed: 6325937]
4. Reeve AE, Housiaux PJ, Gardner RJ, Chewings WE, Grindley RM, Millow LJ. Loss of a Harvey ras allele in sporadic Wilms' tumour. Nature. 1984; 309:174–6. [PubMed: 6325938]
5. Satoh Y, Nakadate H, Nakagawachi T, et al. Genetic and epigenetic alterations on the short arm of chromosome 11 are involved in a majority of sporadic Wilms' tumours. Br J Cancer. 2006; 95:541–7. [PubMed: 16909133]
6. Ali IU, Lidereau R, Theillet C, Callahan R. Reduction to homozygosity of genes on chromosome 11 in human breast neoplasia. Science. 1987; 238:185–8. [PubMed: 3659909]
7. Fearon ER, Feinberg AP, Hamilton SH, Vogelstein B. Loss of genes on the short arm of chromosome 11 in bladder cancer. Nature. 1985; 318:377–80. [PubMed: 2999610]
8. Weston A, Willey JC, Modali R, et al. Differential DNA sequence deletions from chromosomes 3, 11, 13, and 17 in squamous-cell carcinoma, large-cell carcinoma, and adenocarcinoma of the human lung. Proc Natl Acad Sci U S A. 1989; 86:5099–103. [PubMed: 2567993]
9. Lee JH, Kavanagh JJ, Wharton JT, Wildrick DM, Blick M. Allele loss at the c-Ha-ras1 locus in human ovarian cancer. Cancer Res. 1989; 49:1220–2. [PubMed: 2917352]
10. Rainier S, Johnson LA, Dobry CJ, Ping AJ, Grundy PE, Feinberg AP. Relaxation of imprinted genes in human cancer. Nature. 1993; 362:747–9. [PubMed: 8385745]
11. Schwienbacher C, Angioni A, Scelfo R, et al. Abnormal RNA expression of 11p15 imprinted genes and kidney developmental genes in Wilms' tumor. Cancer Res. 2000; 60:1521–5. [PubMed: 10749116]
12. Scelfo RA, Schwienbacher C, Veronese A, et al. Loss of methylation at chromosome 11p15.5 is common in human adult tumors. Oncogene. 2002; 21:2564–72. [PubMed: 11971191]
13. Poirier K, Chalas C, Tissier F, et al. Loss of parental-specific methylation at the IGF2 locus in human hepatocellular carcinoma. J Pathol. 2003; 201:473–9. [PubMed: 14595760]
14. Haruta M, Arai Y, Sugawara W, et al. Duplication of paternal IGF2 or loss of maternal IGF2 imprinting occurs in half of Wilms tumors with various structural WT1 abnormalities. Genes Chromosomes Cancer. 2008; 47:712–27. [PubMed: 18464243]
15. Vu TH, Chuyen NV, Li T, Hoffman AR. Loss of imprinting of IGF2 sense and antisense transcripts in Wilms' tumor. Cancer Res. 2003; 63:1900–5. [PubMed: 12702581]
16. Sparago A, Russo S, Cerrato F, et al. Mechanisms causing imprinting defects in familial Beckwith-Wiedemann syndrome with Wilms' tumour. Hum Mol Genet. 2007; 16:254–64. [PubMed: 17158821]
17. Diaz-Meyer N, Day CD, Khatod K, et al. Silencing of CDKN1C (p57KIP2) is associated with hypomethylation at KvDMR1 in Beckwith-Wiedemann syndrome. J Med Genet. 2003; 40:797–801. [PubMed: 14627666]
18. Satoh A, Toyota M, Ikeda H, et al. Epigenetic inactivation of class II transactivator (CIITA) is associated with the absence of interferon-γ-induced HLA-DR expression in colorectal and gastric cancer cells. Oncogene. 2004; 23:8876–86. [PubMed: 15467734]
19. Gallagher E, Mc Goldrick A, Chung WY, et al. Gain of imprinting of SLC22A18 sense and antisense transcripts in human breast cancer. Genomics. 2006; 88:12–7. [PubMed: 16624517]

20. Bjornsson HT, Brown LJ, Fallin MD, et al. Epigenetic specificity of loss of imprinting of the IGF2 gene in Wilms tumors. J Natl Cancer Inst. 2007; 99:1270–3. [PubMed: 17686827]
21. Sun FL, Dean WL, Kelsey G, Allen ND, Reik W. Transactivation of Igf2 in a mouse model of Beckwith-Wiedemann syndrome. Nature. 1997; 389:809–15. [PubMed: 9349812]
22. Fu H, Tie Y, Xu C, et al. Identification of human fetal liver miRNAs by a novel method. FEBS Lett. 2005; 579:3849–54. [PubMed: 15978578]
23. Negrini M, Ferracin M, Sabbioni S, Croce CM. MicroRNAs in human cancer: from research to therapy. J Cell Sci. 2007; 120:1833–40. [PubMed: 17515481]
24. Esquela-Kerscher A, Slack FJ. Oncomirs—microRNAs with a role in cancer. Nat Rev Cancer. 2006; 6:259–69. [PubMed: 16557279]
25. Calin GA, Croce CM. MicroRNA signatures in human cancers. Nat Rev Cancer. 2006; 6:857–66. [PubMed: 17060945]
26. Kort EJ, Farber L, Tretiakova M, et al. The E2F3-Oncomir-1 axis is activated in Wilms' tumor. Cancer Res. 2008; 68:4034–8. [PubMed: 18519660]
27. Fornari F, Gramantieri L, Ferracin M, et al. MiR-221 controls CDKN1C/p57 and CDKN1B/p27 expression in human hepatocellular carcinoma. Oncogene. 2008; 27:5651–61. [PubMed: 18521080]
28. Jeffers JR, Parganas E, Lee Y, et al. Puma is an essential mediator of p53-dependent and -independent apoptotic pathways. Cancer Cell. 2003; 4:321–8. [PubMed: 14585359]
29. Shimizu M, Shirakami Y, Sakai H, et al. EGCG inhibits activation of the insulin-like growth factor (IGF)/IGF-1 receptor axis in human hepatocellular carcinoma cells. Cancer Lett. 2008; 262:10–8. [PubMed: 18164805]
30. Lin SB, Hsieh SH, Hsu HL, Lai MY, Kan LS, Au LC. Antisense oligodeoxynucleotides of IGF-II selectively inhibit growth of human hepatoma cells overproducing IGF-II. J Biochem. 1997; 122:717–22. [PubMed: 9399573]
31. Nakano K, Vousden KH. PUMA, a novel proapoptotic gene, is induced by p53. Mol Cell. 2001; 7:683–94. [PubMed: 11463392]
32. Yu J, Zhang L, Hwang PM, Kinzler KW, Vogelstein B. PUMA induces the rapid apoptosis of colorectal cancer cells. Mol Cell. 2001; 7:673–82. [PubMed: 11463391]
33. Bouillet P, Strasser A. BH3-only proteins—evolutionarily conserved proapoptotic Bcl-2 family members essential for initiating programmed cell death. J Cell Sci. 2002; 115:1567–74. [PubMed: 11950875]
34. Guled M, Lahti L, Lindholm PM, et al. CDKN2A, NF2, and JUN are dysregulated among other genes by miRNAs in malignant mesothelioma—a miRNA microarray analysis. Genes Chromosomes Cancer. 2009; 48:615–23. [PubMed: 19396864]
35. Elmen J, Lindow M, Schutz S, et al. LNA-mediated microRNA silencing in non-human primates. Nature. 2008; 452:896–9. [PubMed: 18368051]
36. Krutzfeldt J, Rajewsky N, Braich R, et al. Silencing of microRNAs *in vivo* with 'antagomirs'. Nature. 2005; 438:685–9. [PubMed: 16258535]

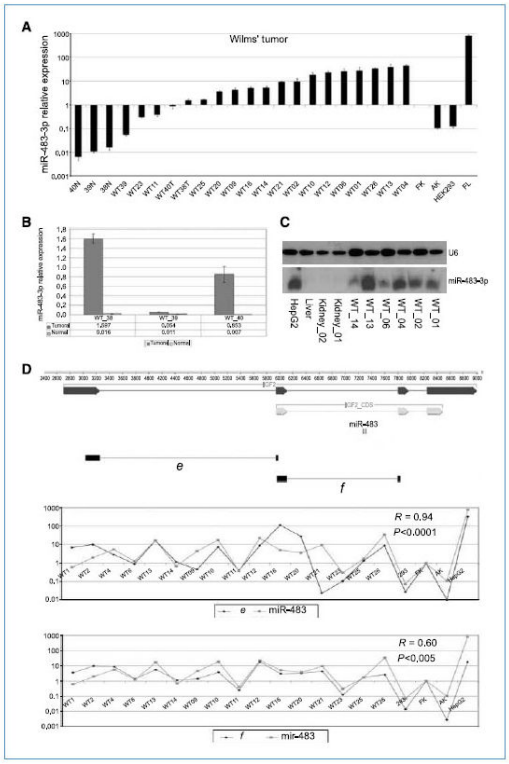

Figure 1.

miR-483-3p and *IGF2* expression in Wilms' tumor. A, *miR-483-3p* relative expression analysis by quantitative real-time PCR on 19 samples of primary Wilms' tumor, 3 adjacent non-tumoral tissues, fetal kidney, cell line HEK293, and fetal liver tissue. Each sample data was normalized to the endogenous reference *RNU6B* and related to the fetal kidney (calibrator) miR-483-3p expression ($2^{-\Delta\Delta Ct}$ method). B, different expressions from normal to tumoral tissue were pointed out in samples (WT_38, WT_39, and WT_40). C, Northern blot analysis of *miR-483-3p* and *RNU6B* in six Wilms' tumor samples, two normal adult kidneys, one normal adult liver, and a HepG2 cell line. D, genomic structure of *IGF2* gene (dark gray arrows) from the reference sequence AF517226; coding sequence (light gray arrows); *miR-483* is indicated in the second *IGF2* intron. Black bars (*e* and *f*) show the cDNA-amplified regions used to analyze *IGF2* expression that was compared with the *miR-483-3p* expression in panels immediately below. *IGF2* expression data were normalized on RNA *18S* and related to *IGF2* fetal kidney expression ($2^{-\Delta\Delta Ct}$). *R*, correlation coefficients; *P*, *P* values.

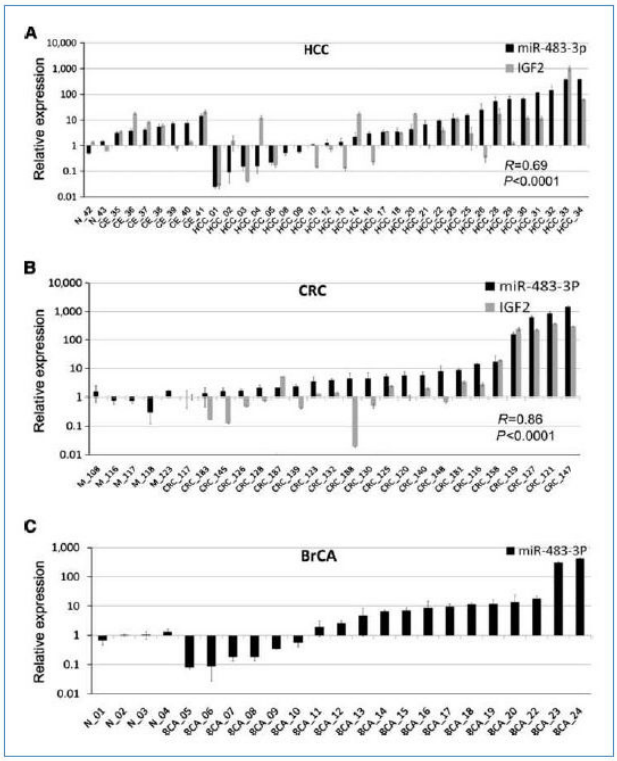

Figure 2.

miR-483-3p and *IGF2* expression in adult human cancers. *miR-483-3p* relative expression by quantitative real-time RT-PCR. The expression of *miR-483-3p* was normalized to the endogenous gene *RNU6B* (black bars) whereas the expression of *IGF2* was normalized in *18S* RNA (gray bars). Expression data were related to the average expression of normal samples of each tissue ($2^{-\Delta\Delta Ct}$ method). Expression of the locus *IGF2/miR-483-3p* was investigated in (A) 27 hepatocarcinomas and 7 non-tumoral cirrhotic livers (CE), which were related to 2 normal liver tissue samples, the positive correlation between *IGF2* and *miR-483-3p* is indicated ($R = 0.69$, $P < 0.0001$); B, 22 colorectal cancer samples were related to 5 normal colon mucosa tissues, the positive correlation between *IGF2* and *miR-483-3p* is indicated ($R = 0.86$, $P < 0.0001$); C, 19 breast cancer and 4 normal breast tissue samples were tested for the expression of *miR-483-3p*.

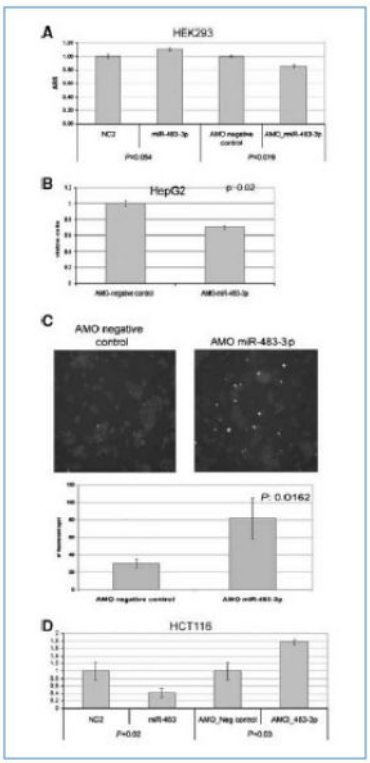

Figure 3.

AMO-483-3p induces cell death. A, cell viability measured by the MTT assay in HEK293 cells. Each value represents the average absorbance ± SD from three different experiments. The differences between miR-483-3p versus negative control 2 ($P = 0.002$), and AMO_miR-483-3p versus AMO negative control ($P = 0.03$) were both statistically significant. B, cell viability of HepG2 cells at 48 h following transfection of AMO-miR-483-3p or AMO negative control. Each value represents the average ± SD from three different experiments ($P = 0.02$ on AMO_miR-483-3p versus AMO negative control) and related to control data. C, terminal deoxynucleotidyl transferase–mediated dUTP nick end labeling staining of HepG2 cells after transfection of AMO-negative control or AMO miR-483-3p. Cells were stained 24 h after transfection. Underneath the images, the average number of fluorescent spots is shown: data in each column represents the average ± SD of fluorescent spots from three independent fields ($P = 0.0162$). D, caspase 3/7 activity in HCT116 cells transfected with miR-483-3p, anti-miR-483-3p AMO, or negative controls; after 24 h, cells were treated with Nutlin-3 (5 μmol/L) for an additional 6 h.

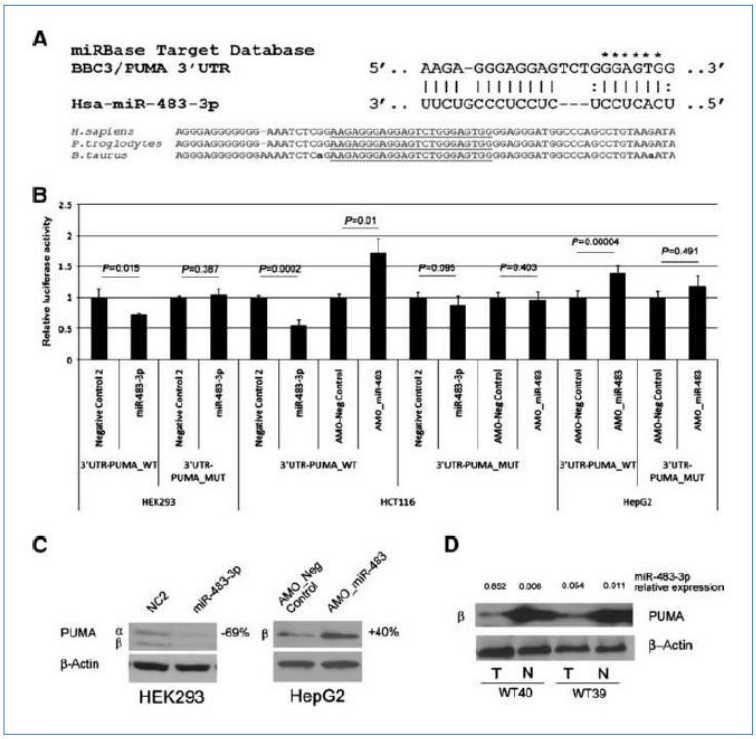

Figure 4.

BBC3/PUMA is target of *miR-483-3p*. A, putative binding site of *miR-483-3p* in PUMA 3′UTRs (miRBase Target Database). Asterisks, nucleotides substituted in *miR-483-3p* predicted target site to perform luciferase assay (GGAGT>AATTA). B, PUMA 3′UTRs regulate luciferase activity dependent on *miR-483-3p* in HEK293, HCT116, and HepG2 cell lines (WT, wild-type; MUT, mutant; *P*, *P* value). Firefly luciferase activity was normalized on Renilla luciferase activity of the cotransfected pRL-TK vector. C, Western blot analysis of PUMA after *miR-483-3p* transfection in HEK293 and HepG2 cell line; the α (23 kDa) and β (18 kDa) isoforms are indicated. Cells were collected after 48 h of miRNA transfection. D, Western blot analysis of PUMA in Wilms' tumor samples (T) and matched normal tissues (N).

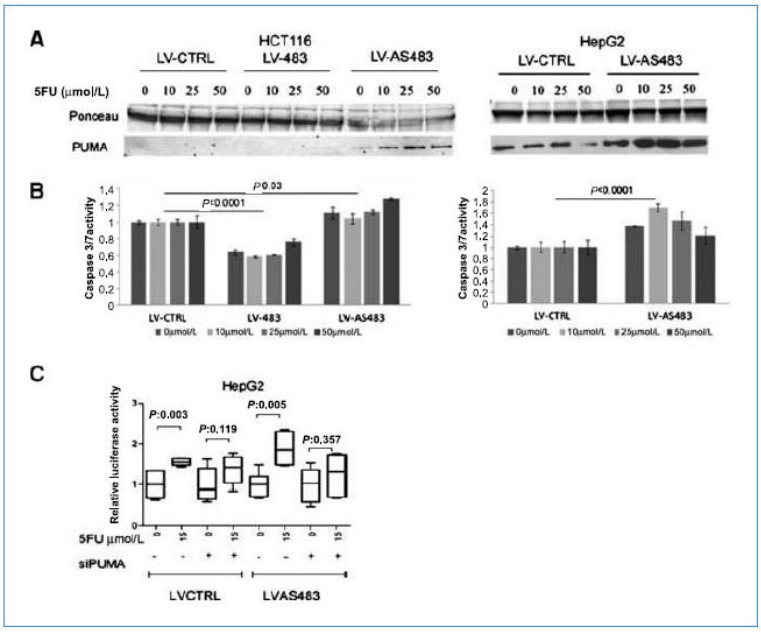

Figure 5.

Stable cell lines overexpressing anti–miR-483-3p are more sensitive to apoptosis stimuli. HCT116 cells overexpressing the *miR-483-3p* (LV-483) or the anti–*miR-483-3p* (LV-AS483) and HepG2 cells overexpressing the anti–miR-483-3p were treated with different concentrations of 5FU. LV-CTRL indicates stable cell line with the empty vector. A, Western blot analysis reveals an increment of PUMA protein levels only in the LV-AS483 cells. B, caspase 3/7 activity was decreased in LV-483 cells and increased in LV-AS483 when compared with LV-CTRL cells. Data were normalized on LV-CTRL cells. C, relative caspase 3/7 activity in HepG2-LV-CTRL and LV-AS483 after treatment with 5FU and siPUMA (+) or siRNA scramble (−). Data were normalized on the average caspase activity of HepG2-LV-CTRL cells.

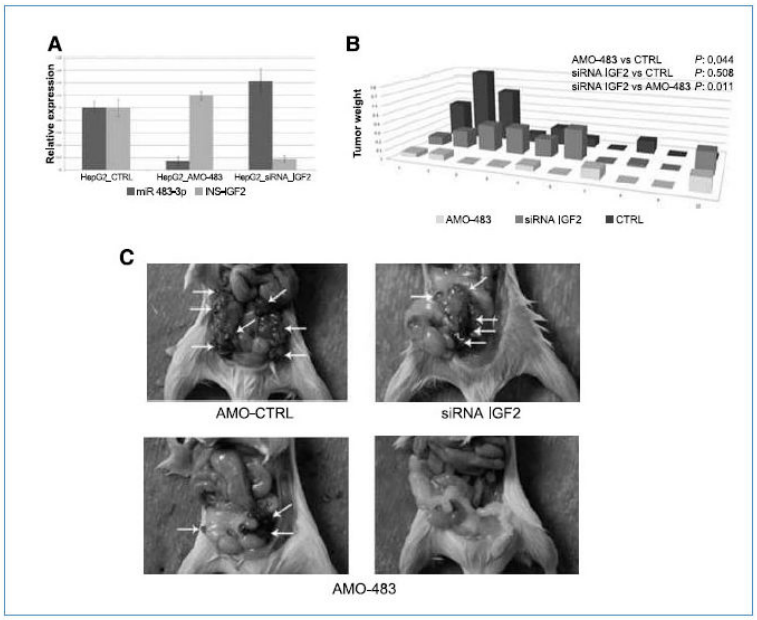

Figure 6.

AMO-483-3p reduces tumors induced by HepG2 cells *in vivo*. A, a qRT-PCR analysis to verify the reduction of *miR-483-3p* and *IGF2* mRNA after transfection of AMO-483-3p or siRNA anti-*IGF2* in HepG2 cells. B, tumors from each mouse were weighed: a significant difference ($P < 0.05$) in tumor weights was found between AMO-483-3p and AMO negative control transfected (CTRL) cells, between siRNA IGF2 and AMO-483-3p ($P < 0.02$), but not between siRNA *IGF2* and AMO-CTRL–transfected HepG2 cells ($P > 0.5$). C, appearance of intraperitoneal HepG2 induced tumors in NOD-SCID mice (white arrows, tumor formations).